














A Framework for Jointly Assessing and Reducing Imaging Artefacts Automatically Using Texture Analysis and Total Variation Optimisation for Improving Perivascular Spaces Quantification in Brain Magnetic Resonance Imaging

Jose Bernal¹(✉) , Maria Valdés-Hernández¹ , Lucia Ballerini¹ ,
Javier Escudero² , Angela C. C. Jochems¹ , Una Clancy¹ ,
Fergus N. Doubal¹ , Michael S. Stringer¹ , Michael J. Thrippleton¹ ,
Rhian M. Touyz³ , and Joanna M. Wardlaw¹ 

¹ Centre for Clinical Brain Sciences, University of Edinburgh, Edinburgh, UK
jose.bernal@ed.ac.uk

² Institute for Digital Communications, University of Edinburgh, Edinburgh, UK

³ Institute of Cardiovascular and Medical Sciences, University of Glasgow,
Glasgow, UK

Abstract. Perivascular spaces are fluid-filled tubular spaces that follow the course of cerebral penetrating vessels, thought to be a key part in the brain's circulation and glymphatic drainage system. Their enlargement and abundance have been found associated with cerebral small vessel disease. Thus, their quantification is essential for establishing their relationship with neurological diseases. Previous works in the field have designed visual rating scales for assessing the presence of perivascular spaces and proposed segmentation techniques to reduce flooring and ceiling effects of qualitative visual scales, processing times, and inter-observer variability. Nonetheless, their application depends on the acquisition quality. In this paper, we propose a framework for improving perivascular spaces quantification using both texture analysis and total variation filtering. Texture features were considered for evaluating the image quality and determining automatically whether filtering was needed. We tested our work using data from a cohort of patients with mild stroke ($n = 60$) with different extents of small vessel disease features and image quality. Our results demonstrate the potential of our proposal for improving perivascular spaces assessments.

Keywords: Perivascular spaces · Cerebral small vessel disease · Image enhancement · Imaging artefact reduction · Brain magnetic resonance imaging

1 Introduction

Perivascular spaces (PVS), also referred to as Virchow-Robin spaces, are fluid-filled tubular spaces that follow the course of deep cerebral perforating vessels, thought to play a role in cerebral hemodynamics and interstitial fluid drainage [3, 7, 9, 22]. In magnetic resonance imaging, these spaces are visible on T1-w or T2-w as thin linear or round structures of cerebrospinal fluid like signal located in deep grey matter and white matter [21]. Although they may be normal at any age, their enlarged appearance has been found associated with ageing, hypertension, features of cerebral small vessel disease [4, 9, 22]; cognitive impairment [1, 14]; and active inflammation [17]. Therefore, their precise quantification may help to further validate their use as a neuroimaging feature for brain diseases and shed light on pathophysiological mechanisms of stroke, dementia, and other neurological disorders.

Visual rating scales accounting for the overall burden of PVS [14, 16] have been used in clinical practice and considered the gold standard in assessing PVS, but are prone to inter-observer variability. Semi-automatic (e.g. thresholding) [8, 20] and fully-automatic [3] schemes to segment PVS reduce both processing time and subjectivity, but their application is subject to the quality of the acquisitions [4, 12]. We hypothesise that image enhancement can help to reduce imaging artefacts and potentially improve PVS segmentation.

The total variation optimisation framework is a widespread strategy for denoising [18], reconstruction [13], and artefact suppression [6]. In the work of Block *et al.* [6], the authors commented that a key property of the total variation seminorm is that it reacts to the extent of artefacts: the higher the distortion degree, the higher the value of the total variation component. Therefore, its minimisation leads to artefact suppression. This particular asset makes such a strategy appealing as it could reduce imaging artefacts and perhaps lead to improved PVS quantification.

In this research work, we design a framework to identify magnetic resonance images corrupted by imaging artefact and examine whether the total variation framework permits reducing these artefacts while retaining clinically-relevant information. We use data from a cohort of patients with mild stroke with varied extents of small vessel disease features. The contributions of this work are threefold: 1) we propose a fully functional framework for improving the assessment of PVS; 2) we show qualitatively that our pipeline correctly identifies noisy images and reduces visual artefacts on them; 3) we show quantitatively that, when images are noisy, the relationship between computational measurements and visual clinical ratings is stronger when filtered scans are used instead of the original acquisitions.

2 Materials and Methods

Our processing framework consists of three steps, as shown in Fig. 1. First, we extract texture features to determine whether image requires filtering or not.

Second, if artefact reduction is needed, we use the total variation optimisation framework. Third, we segment PVS in both filtered and unfiltered scans in two regions of interest (basal ganglia and centrum semiovale) for each patient in the sample. To validate our proposal, we determine whether quantitative PVS computational measures extracted from filtered scans relate better (or not) to clinical visual scores when images are noisy. Details of each step are provided in the following sections.

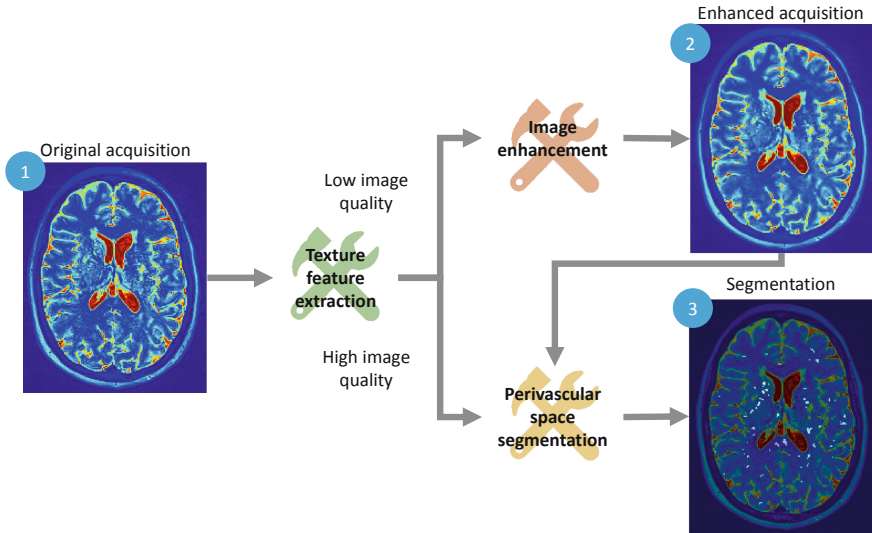


Fig. 1. High-level scheme of our processing pipeline per input volume. The inputs are T2-w scans. First, examined whether the scans need filtering or not using texture analysis. Second, we filter the scan, in case it is needed. Third, we segment perivascular spaces using a fully validated strategy.

2.1 Subjects, Imaging, and Clinical Scores

We used data from an ongoing prospective study (The Mild Stroke Study 3: ISCTRN 12113543) of patients with a recent mild stroke ($n = 60$; 24 women; median age 69 years [IQR 58–75]; age range 40 to 85 years) with a varied burden of neuroimaging features of small vessel disease. Ethical approval for this study was obtained from South East Scotland Research Ethics Committee (Ref 18/SS/0044) on 31/05/2018. NHS Lothian Research & Development approved this study on 31/05/2018 (Ref 2018/0084). Imaging was carried out on a 3T MRI scanner (MAGNETOM Prisma, Siemens Healthcare, Erlangen, Germany) using a 32-channel head receive coil. Structural MRI at baseline consisted of 3D sagittal MPRAGE T1-w imaging (TR/TE/TI = 2500/4.37/1100 ms, 7° flip angle, 1 mm isotropic acquired resolution, 25.6×25.6 cm field of view), 3D sagittal SPACE

fluid-attenuated inversion recovery imaging (TR/TE/TI = 5000/388/1800 ms, 1 mm isotropic acquired resolution, 25.6×25.6 cm field of view), and 3D axial SPACE T2-w imaging (TR/TE = 3200/408 ms, $0.94 \times 0.94 \times 0.90$ mm acquired resolution, 24.0×24.0 cm field of view).

We considered a visual clinical rating recorded at baseline to account for the presence and extent of enlarged PVS in the basal ganglia and centrum semiovale [15]. An experienced neuroradiologist rated PVS on T2-w images of the whole sample. The distribution of such scores in our cohort is depicted in Fig. 2.

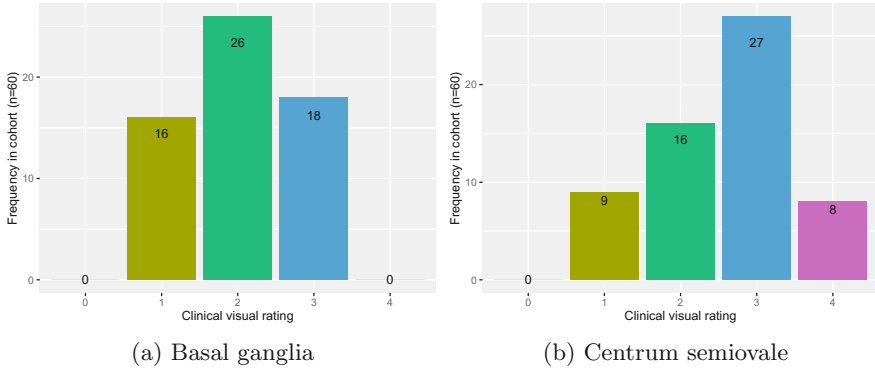


Fig. 2. Distribution of clinical visual ratings accounting for the presence and abundance of perivascular spaces in patients in our cohort. On the left, visual scores for basal ganglia. On the right, visual scores for centrum semiovale. The number inside each bar corresponds to the number of patients in each category.

2.2 Texture-Based Image Quality Classification

While filtering noisy scans may reduce false positives, it may reduce true positives in clean ones. Our first step consists of automatically determining whether the input scan requires being filtered or not. For that, we extracted the six Haralick texture features indicative of variability/homogeneity (i.e. energy, contrast, correlation, homogeneity, entropy and variance) [11] from the acquired T2-w image and used logistic regression to predict whether filtering was needed or not. A trained analyst blind to our classification process classified the images into “noisy” and “clean/smooth”.

2.3 Segmentation of Perivascular Spaces

We segmented tubular-like structures in T2-w images in two regions of interest, centrum semiovale and basal ganglia, using the method described in Ballerini *et al.* [2]. The method consists of image enhancement, thresholding, and connected component analysis. We applied the three-dimensional Frangi filter [10] to enhance tubular geometrical objects, such as PVS. We computed the “vesselness”

of each voxel at scales from 0.4 and 0.8 and a step of 0.2, combined responses for each filter, and thresholded them using default parameters ($\alpha = 0.5$, $\beta = 0.5$ and $C = 500$). The connected component analysis step consisted of identifying 3D voxel clusters with lengths between 3 and 50 mm and filtering out large candidates (volume higher than 1000 voxels) as they potentially corresponded to white matter hyperintensities. Further details of the method are described in full in [2].

We defined PVS count as the number of connected components in the segmented images and volume as the total number of voxels classified as PVS multiplied by the voxel size and divided by the intracranial volume.

2.4 A Total Variation Optimisation Framework for Reducing Imaging Artefacts

Block *et al.* [6] explained that the total variation increases with the extent of truncation artefacts and showed that its minimisation could suppress imaging artefacts in synthetic and real magnetic resonance images. We built our image filtering framework on that premise as follows. Let $Y \in \mathbb{R}^{N \times M \times L}$ be the original acquisition, our task consists of regressing $X \in \mathbb{R}^{N \times M \times L}$ such that the following cost function is minimised

$$\lambda \|X\|_{\text{TV}} + \frac{1}{2} \|HX - Y\|_2^2, \quad (1)$$

where H is a transformation matrix, λ is a weighting parameter than controls the filter strength, and $\|X\|_{\text{TV}} = \sum \|\nabla X\|$. This formulation permits obtaining an artefact-reduced image, due to the total variation component, which appears similar to the original one, due to the fidelity term. We optimised the cost function iteratively by updating X according to the following formula:

$$X^{(i+1)} = X^{(i)} + \gamma^{(i)} \cdot \left[\lambda \cdot \nabla \left(\frac{\nabla X^{(i)}}{\|\nabla X^{(i)}\|} \right) + H^\top (HX^{(i)} - Y) \right], \quad (2)$$

where X^0 is the starting point, $\gamma^{(i)}$ determines the step in the direction of the gradient at the i -th iteration, and \top represents the transpose operation. We found the most suitable value for $\gamma^{(i)}$ using the line search algorithm. Note that the number of iterations and the parameter λ need to be tuned up in such a way the output preserves clinically relevant structures, such as PVS, while smoothing regions affected by artefacts. As we carried out our filtering in the image domain, the matrix H is the identity matrix.

2.5 Validation Against Clinical Parameters

We applied ordinal logistic regression to assess whether computational measures could predict clinical visual scores, the Kruskal-Wallis test to determine whether patient grouped according to visual scores presented similar quantitative measures, and the polyserial correlation to calculate the degree of correlation between visual and computational values. We carried out our statistical analyses using RStudio v1.1.456 with R v3.5.1.

3 Results

3.1 Qualitative Results

Visual examples of filtering with three different filter strengths (in particular, $\lambda = 2, 5$ and 10) are presented in Fig. 3. The higher the weight of the total variation component, the smoother the output. This parameter is critical in our assessments as a low value for λ results in noisy scans in which PVS are still visible while a high value results in smooth scans in which noise is reduced but many PVS may be discarded. By visually examining scans filtered with different parameter values, we found out experimentally that a value $\lambda = 2$ and 100 iterations led to acceptable filtering results for the entire cohort. Of note, such an assessment does not ensure these parameters lead to the best association or correlation between clinical visual scores and PVS quantification.

Segmentation examples before and after filtering on noisy and “clean” scans are shown in Fig. 4. In noisy scans, filtering tends to decrease the number of detected PVS, possibly due to a reduction of false positives. Filtering “clean” scans resulted in a reduction on both PVS count and volume. Since these images did not exhibit visual artefacts, this outcome suggests underestimation and justifies the use of the texture-based image quality classification strategy.

3.2 Texture-Based Image Quality Classification Results

We determined whether to filter an input scan or not based on its textures. The process consisted of three steps. First, we split our original dataset into training (67%) and testing (33%). We divided in such a way the ratio of “noisy” images in each dataset was the same (30%). Second, we trained seven logistic regression models: six using Haralick feature independently and one combining them all. We tune parameters using a 10-fold cross-validation strategy. Third, we tested the performance of each model on the test set in terms of the area under the curve. The combination of all texture features resulted in better classification values (AUC = 88.80%) compared to independent approaches (AUC: Energy 75.00%; Contrast 67.86%; Correlation 66.67%; Homogeneity 55.95%; Entropy 71.43%; Variability 70.24%). From hereon, we used the logistic regression model using all textures to determine whether to filter input scans (Intercept: $\beta = -41.32$ (CI $-198.48, 95.74$), $p = 0.56$; Energy: $\beta = -559.15$ (CI $-1216.58, -169.76$), $p < 0.05$; Contrast: $\beta = -11.42$ (CI $-26.73, -1.96$), $p = 0.6$; Correlation: $\beta = 25.72$ (CI $-49.91, 118.83$), $p = 0.52$; Homogeneity: $\beta = -0.66$ (CI $-5.75, 3.95$), $p = 0.78$; Entropy: $\beta = 2.25$ (CI $-0.88, 6.48$), $p = 0.21$; Variance: $\beta = -0.01$ (CI $-0.05, 0.02$), $p = 0.39$). Of note, this equation is suitable for this specific acquisition protocol and, thus, it needs to be readjusted for another one.

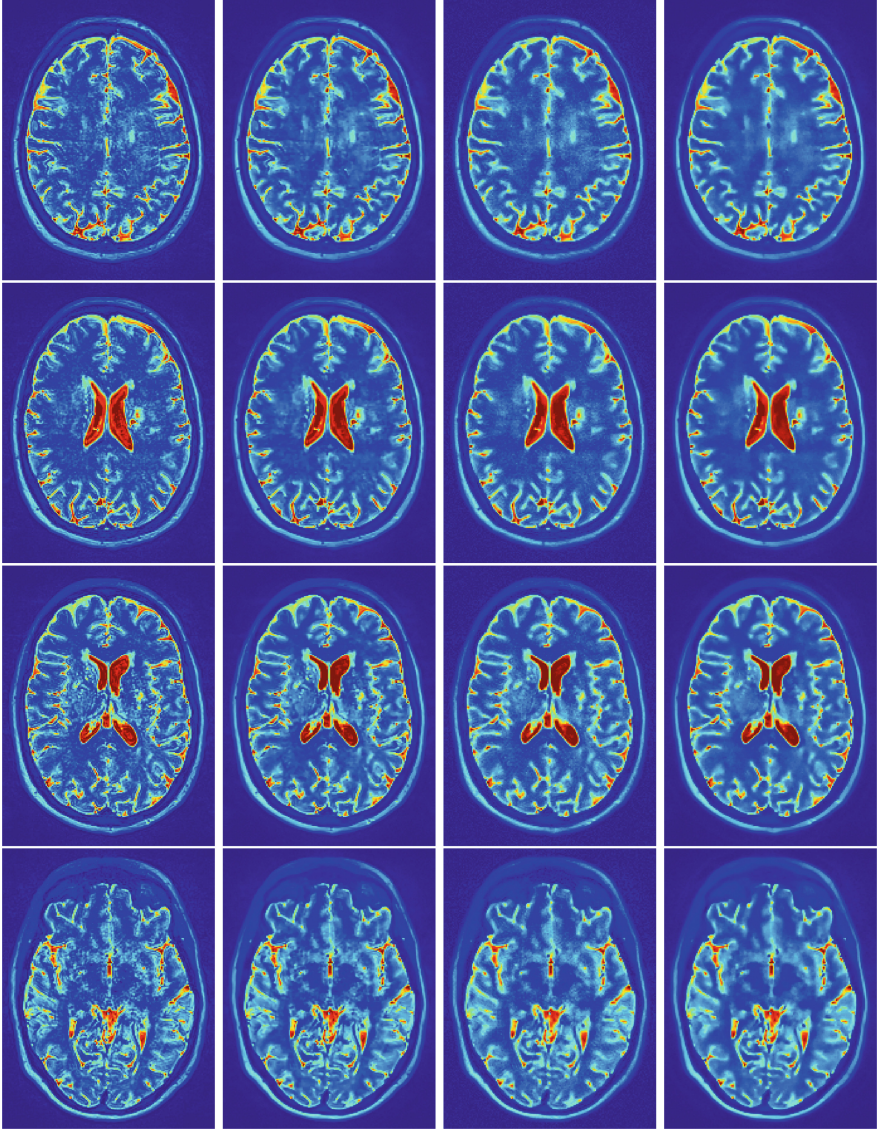


Fig. 3. Artefact reduction on T2-w scans. From left to right, original scan and filtered ones using $\lambda = 2, 5, 10$ and 100 iterations. Of note, the higher the lambda, the smoother the scan. Recall that perivascular spaces appear as thin linear or round structures of cerebrospinal fluid like signal located in deep grey matter and white matter.

3.3 Validation Against Clinical Visual Rating

We determined the suitability of the filtering technique by examining the strength of the relationship between quantitative scores and clinical

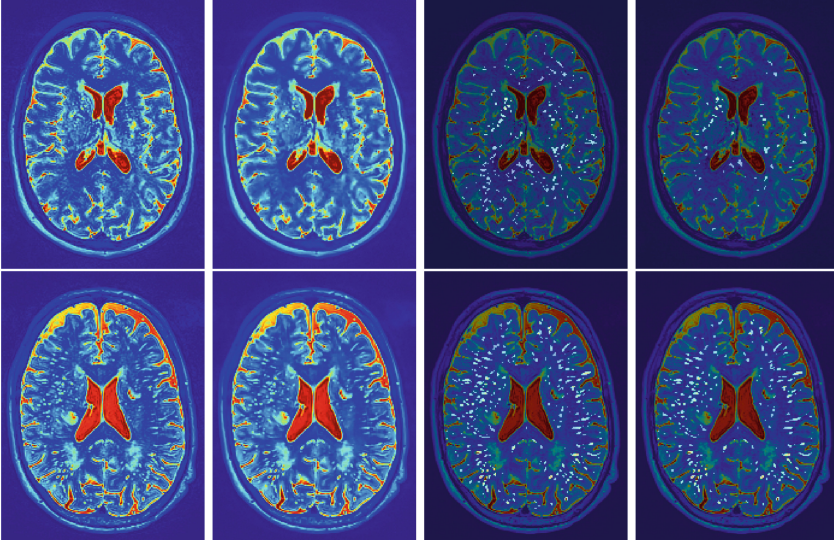


Fig. 4. Effect of artefact reduction on perivascular space segmentation. From left to right, original scan and filtered scan using $\lambda = 2$ and 100, segmentation results using the original acquisition and segmentation results using filtered acquisition. Recall that perivascular spaces appear as thin linear or round structures of cerebrospinal fluid like signal located in deep grey matter and white matter.

visual ratings versus when omitted. We hypothesised that the strength of such relationships improves after filtering.

We used ordinal logistic regression to examine whether clinical visual scores could predict the count and volume of PVS extracted from original and filtered scans. The regression results are condensed in Table 1.

While R^2 values were approximately 13% and 40% for both count and volume of PVS in the basal ganglia in original scans, they increased to 30% and 47% for the same measurements when filtered. In all measurements from the basal ganglia, the computational scores were strong predictors of the clinical visual scores and were positively associated with them (Original: $\beta_{\text{count}} = 0.01$ (CI 0.00, 0.02), $p < 0.01$ and $\beta_{\text{volume}} = 20.28$ (CI 12.11, 31.54), $p < 0.001$; Filter all: $\beta_{\text{count}} = 0.02$ (CI 0.01, 0.04), $p < 0.001$ and $\beta_{\text{volume}} = 35.92$ (CI 21.25, 50.59), $p < 0.001$; Proposed scheme: $\beta_{\text{count}} = 0.02$ (CI 0.01, 0.03), $p < 0.001$ and $\beta_{\text{volume}} = 34.99$ (CI 21.14, 48.83), $p < 0.001$). In the centrum semiovale, the relationships were not as evident as in the basal ganglia before filtering. While in most of the cases, no significant relationships were observed (Original: $\beta_{\text{count}} = 0.00$ (CI 0.00, 0.00), $p = 0.16$ and $\beta_{\text{volume}} = 0.76$ (CI 0.00, 1.52), $p = 0.05$; Filter all: $\beta_{\text{count}} = 0.00$ (CI 0.00, 0.00), $p = 0.26$), our proposed selective filtering scheme resulted in significant ones ($\beta_{\text{count}} = 0.00$ (CI 0.00, 0.00), $p < 0.05$ and $\beta_{\text{volume}} = 2.48$ (CI 1.33, 3.64), $p < 0.001$).

Table 1. Ordinal logistic regression with quantitative measures of PVS as predictor and clinical visual scores as outcome variable. We consider the count and volume as quantitative PVS measurements. The R^2 correspond to the Nagelkerke’s R^2 . CI: confidence interval. BG: basal ganglia. CSO: centrum semiovale.

	Variable	Original				Filter all				Proposed selective filtering						
		R^2 (%)	β	95% CI		P-value	R^2 (%)	β	95% CI		P-value	R^2 (%)	β	95% CI		P-value
BG	Count	12.96	0.01	0.00, 0.02		9.20e-03	29.98	0.02	0.01, 0.04		1.14e-04	29.38	0.02	0.01, 0.03		1.18e-04
	Volume	39.48	20.28	12.11, 31.54		2.46e-05	46.84	35.92	21.25, 50.59		1.59e-06	44.98	34.99	21.14, 48.83		7.27e-07
CSO	Count	0.73	0.00	-0.00, 0.00		1.62e-01	2.53	0.00	-0.00, 0.00		2.58e-01	11.03	0.00	0.00, 0.00		1.62e-02
	Volume	7.55	0.76	-0.00, 1.52		5.02e-02	22.38	2.15	0.91, 3.39		6.67e-04	34.81	2.48	1.33, 3.64		2.37e-05

We applied the Kruskal-Wallis test to determine whether patients with similar visual rating presented similar computational PVS count and volume. We compared the results obtained before and after filtering. The outputs are condensed in Table 2. Both count and volume were significantly different for patients with different PVS visual scores in the basal ganglia regardless of whether all scans were filtered (Count: $\chi^2 = 14.74$, $df = 2$, $p < 0.001$ and Volume: $\chi^2 = 27.35$, $df = 2$, $p < 0.001$), some of them based on their predicted image quality (Count: $\chi^2 = 15.76$, $df = 2$, $p < 0.001$ and Volume: $\chi^2 = 25.67$, $df = 2$, $p < 0.001$), or not (Count: $\chi^2 = 6.58$, $df = 2$, $p < 0.05$ and Volume: $\chi^2 = 22.19$, $df = 2$, $p < 0.001$). The case was not the same when patients were grouped based on their PVS visual scores in the centrum semiovale. We found significant differences in both measurements when using our texture-based selective filtering in both count (Count: $\chi^2 = 16.88$, $df = 2$, $p < 0.001$ and Volume: $\chi^2 = 24.11$, $df = 2$, $p < 0.001$). In the rest of the cases, we only found significant variations when considering the overall PVS volume computed from both unfiltered ($\chi^2 = 11.64$, $df = 2$, $p < 0.01$) and filtered data (Filter all: $\chi^2 = 18.16$, $df = 2$, $p < 0.001$). Of note, in all cases, the differences between patient groups were more noticeable (i.e. lower p -value) using measures computed from enhanced scans.

We considered the polyserial correlation to quantify the correlation between categorical visual scores and quantitative PVS measures. The results are presented in Table 2. The correlation between computational measurements and visual scores increased consistently after filtering. In the basal ganglia, correlation results went from $\rho_{\text{Count}} = 0.38$ (CI 0.35, 0.41) and $\rho_{\text{Volume}} = 0.63$ (CI 0.61, 0.65) when segmenting PVS on raw acquisitions to $\rho_{\text{Count}} = 0.57$ (CI 0.55, 0.59) and $\rho_{\text{Volume}} = 0.70$ (CI 0.68, 0.72) when preprocessing the proposed filtering strategies. Similarly, in the centrum semiovale, the correlation for both count and volume increased from $\rho_{\text{Count}} = -0.10$ (CI -0.13, -0.06) and $\rho_{\text{Volume}} = 0.27$ (CI 0.24, 0.30) to $\rho_{\text{Count}} = 0.14$ (CI 0.10, 0.17) and $\rho_{\text{Volume}} = 0.42$ (CI 0.39, 0.45) when filtering all scans and to $\rho_{\text{Count}} = 0.30$ (CI 0.26, 0.33) and $\rho_{\text{Volume}} = 0.57$ (CI 0.55, 0.60) when using our proposal. Of note, the sign of the correlation between the visual rating and the computational PVS count in the centrum semiovale changed from negative on original scans to positive on filtered scans.

Table 2. Kruskal-Wallis test and polyserial correlation results between quantitative and visual measures of perivascular spaces before and after image filtering. We consider the count and volume as quantitative measurements of the presence of perivascular spaces. CI: confidence interval. BG: basal ganglia. CSO: centrum semiovale.

		Original			Filter all			Proposed selective filtering		
	Variable	Kruskal-Wallis	Correlation		Kruskal-Wallis	Correlation		Kruskal-Wallis	Correlation	
			ρ	95% CI		ρ	95% CI		ρ	95% CI
BG	Count	3.72e-02	0.38	0.35, 0.41	6.29e-04	0.58	0.56, 0.61	3.78e-04	0.57	0.55, 0.59
	Volume	1.51e-05	0.63	0.61, 0.65	1.51e-06	0.70	0.68, 0.72	2.67e-06	0.70	0.68, 0.72
CSO	Count	7.53e-01	-0.10	-0.13, -0.06	7.48e-02	0.14	0.10, 0.17	7.51e-04	0.30	0.26, 0.33
	Volume	8.70e-03	0.27	0.24, 0.30	4.06e-04	0.42	0.39, 0.45	2.37e-05	0.57	0.55, 0.60

4 Discussion

In this paper, we propose a framework for reducing imaging artefacts retrospectively while retaining clinically-relevant biomarkers of small vessel disease, perivascular spaces (i.e. abbreviatedly PVS) in particular. Our framework consisted of three steps: automatic image quality assessment, filtering, and segmentation. First, we automatically examined the quality of the input scans using texture features. If the quality was acceptable, filtering was avoided; otherwise, the data would be processed. Second, distorted images were processed using the total variation optimisation framework to reduce imaging artefacts. Third, we used a previously validated segmentation pipeline to detect and quantify PVS. Although our approach is not the first one enhancing PVS [12], this is the first time that the effect of filtering has been assessed quantitatively using clinical visual ratings.

Evaluation of our pipeline was carried out using three statistic tools to investigate the relationship between clinical visual scores accounting for the PVS presence and extent using two quantitative measurements: count and volume. We inspected these values in two regions of interest of clinical relevance, the basal ganglia and centrum semiovale. First, simple linear regression revealed that filtering led to similar or stronger associations compared to when omitted regardless of the region of interest and the measurement. Second, the Kruskal-Wallis test demonstrated that, in most cases, except for the PVS count in the centrum semiovale, differences between groups of patients were significantly and these differences were more evident when segmenting PVS from filtered scans as opposed to unfiltered ones. Third, the polyserial correlation between clinical visual scores and quantitative measurements before and after filtering showed that visual scores correlated better with quantitative measures computed from filtered scans compared to those of unfiltered ones. In all cases, the use of our automatic image quality assessment strategy resulted in similar or superior performance compared to when filtering all scans or none.

The primary outcomes of the current work are three-fold. First, artefact reduction is necessary to make use of images that would otherwise be discarded due to their level of distortion and to reduce potential false positives. Note that

the former aspect is crucial, more in large-scale studies. For example, 23% of 700 T2-w scans of the Lothian Birth Cohort 1936 were not processed since imaging artefacts hindered their segmentation [4]. We think that imaging enhancement can help to improve the quality of the images, reducing the research waste and adding more confidence to studies results. Second, the total variation framework, which targets truncation and noise artefacts in particular, seems promising and suitable for reducing visual artefacts mainly due to truncation and motion and improving PVS segmentation and quantification. However, our pipeline needs further testing on a larger sample and in cross-sectional and longitudinal studies. Third, the application of such a filtering strategy needs to be applied only to cases in which image quality is low as filtering clean scans might be detrimental.

Our proposal was evaluated on a subsample of a study of mild stroke. Accordingly, we plan to carry out the same assessment on a larger sample to draw stronger conclusions about the pertinence and suitability of imaging enhancement for improving computational methods for studying small vessel disease. The lack of ground truth prevents us from telling with confidence whether filtering is indeed better than omitting it. Nonetheless, we think that a careful statistical analysis looking at the strength of the associations between quantitative computational measurements of PVS and demographics and clinical risk factors could provide us insights on whether the proposal improves the evaluation process or not. Additionally, we selected a useful filter strength qualitatively, not quantitatively. In the future, we will consider alternative image quality classification schemes (e.g. using deep learning [5] or evolutionary algorithms [19], which have proven useful in medical and biomedical analyses) and carry out cross-validation or hold-out tests to systematically determine a suitable value for it. Moreover, the current proposal needs to be tested on other structural and dynamic sequences to examine whether it is suitable not only for improving the segmentation and quantification of PVS, but also other neuroimaging features of small vessel disease.

Acknowledgements. This work is supported by: the UK Dementia Research Institute which receives its funding from DRI Ltd, funded by the UK MRC, Alzheimer’s Society and Alzheimer’s Research UK; the Fondation Leducq Network for the Study of Perivascular Spaces in Small Vessel Disease (16 CVD 05); Stroke Association ‘Small Vessel Disease-Spotlight on Symptoms (SVD-SOS)’ (SAPG 19\100068); The Row Fogo Charitable Trust Centre for Research into Aging and the Brain (MVH) (BRO-D.FID3668413); Stroke Association Garfield Weston Foundation Senior Clinical Lectureship (FND) (TSALECT 2015/04); NHS Research Scotland (FND); British Heart Foundation Edinburgh Centre for Research Excellence (RE/18/5/34216); a British Heart Foundation Chair award (RMT) (CH/12/4/29762); NHS Lothian Research and Development Office (MJT); European Union Horizon 2020, PHC-03-15, project No666881, ‘SVDs@Target’ (MS); Chief Scientist Office of Scotland Clinical Academic Fellowship (UC) (CAF/18/08); Stroke Association Princess Margaret Research Development Fellowship (UC) (2018); MRC Doctoral Training Programme in Precision Medicine (JB); Alzheimer Nederland (ACCJ). The Research MR scanners are supported by the Scottish Funding Council through the Scottish Imaging Network, A Platform for Scientific Excellence (SINAPSE) Collaboration; the 3 T scanner is funded

by the Wellcome Trust (104916/Z/14/Z), Dunhill Trust (R380R/1114), Edinburgh and Lothians Health Foundation (2012/17), Muir Maxwell Research Fund, and the University of Edinburgh. We thank the participants, their families, radiographers at Edinburgh Imaging Facility Royal Infirmary of Edinburgh, and the Stroke Research Network at the University of Edinburgh.

References

1. Arba, F., et al.: Enlarged perivascular spaces and cognitive impairment after stroke and transient ischemic attack. *Int. J. Stroke* **13**(1), 47–56 (2018)
2. Ballerini, L., et al.: Application of the ordered logit model to optimising frangi filter parameters for segmentation of perivascular spaces. *Procedia Comput. Sci.* **90**, 61–67 (2016)
3. Ballerini, L., et al.: Perivascular spaces segmentation in brain MRI using optimal 3D filtering. *Sci. Rep.* **8**(1), 2132 (2018)
4. Ballerini, L., et al.: Computational quantification of brain perivascular space morphologies: Associations with vascular risk factors and white matter hyperintensities. A study in the Lothian Birth Cohort 1936. *NeuroImage Clin.* **25**, 102120 (2020)
5. Bernal, J., et al.: Deep convolutional neural networks for brain image analysis on magnetic resonance imaging: a review. *Artif. Intell. Med.* **95**, 64–81 (2019)
6. Block, K.T., Uecker, M., Frahm, J.: Suppression of MRI truncation artifacts using total variation constrained data extrapolation. *Int. J. Biomed. Imag.* **2008** (2008)
7. Brown, R., et al.: Understanding the role of the perivascular space in cerebral small vessel disease. *Cardiovasc. Res.* **114**(11), 1462–1473 (2018)
8. Descombes, X., et al.: An object-based approach for detecting small brain lesions: application to virchow-robin spaces. *IEEE Trans. Med. Imag.* **23**(2), 246–255 (2004)
9. Francis, F., Ballerini, L., Wardlaw, J.M.: Perivascular spaces and their associations with risk factors, clinical disorders and neuroimaging features: a systematic review and meta-analysis. *Int. J. Stroke* **14**(4), 359–371 (2019)
10. Frangi, A.F., Niessen, W.J., Vincken, K.L., Viergever, M.A.: Multiscale vessel enhancement filtering. In: Wells, W.M., Colchester, A., Delp, S. (eds.) *MICCAI 1998*. LNCS, vol. 1496, pp. 130–137. Springer, Heidelberg (1998). <https://doi.org/10.1007/BFb0056195>
11. Haralick, R.M., Shanmugam, K., Dinstein, I.: Textural features for image classification. *IEEE Trans. Syst. Man Cybern.SMC* **3**(6), 610–621 (1973)
12. Jung, E., et al.: Enhancement of perivascular spaces using densely connected deep convolutional neural network. *IEEE Access* **7**, 18382–18391 (2019)
13. Lustig, M., Donoho, D., Pauly, J.M.: Sparse MRI: the application of compressed sensing for rapid MR imaging. *Magn. Reson. Med. Official J. Int. Soc. Magn. Reson. Med.* **58**(6), 1182–1195 (2007)
14. MacLulich, A., et al.: Enlarged perivascular spaces are associated with cognitive function in healthy elderly men. *J. Neurol. Neurosurg. Psychiatry* **75**(11), 1519–1523 (2004)
15. Potter, G., et al.: Associations of clinical stroke misclassification (‘clinical-imaging dissociation’) in acute ischemic stroke. *Cerebrovasc. Dis.* **29**(4), 395–402 (2010)
16. Potter, G.M., et al.: Cerebral perivascular spaces visible on magnetic resonance imaging: development of a qualitative rating scale and its observer reliability. *Cerebrovasc. Dis.* **39**(3–4), 224–231 (2015)

17. Potter, G.M., et al.: Enlarged perivascular spaces and cerebral small vessel disease. *Int. J. stroke* **10**(3), 376–381 (2015)
18. Rudin, L.I., Osher, S., Fatemi, E.: Nonlinear total variation based noise removal algorithms. *Phys. D Nonlinear Phenom.* **60**(1–4), 259–268 (1992)
19. Smith, S.L., Walker, J.A., Miller, J.F.: Medical Applications of Cartesian Genetic Programming. In: Miller, J. (ed.) *Cartesian Genetic Programming*. Natural Computing Series, pp. 309–336. Springer, Heidelberg (2011). https://doi.org/10.1007/978-3-642-17310-3_11
20. Valdés-Hernández, M., et al.: Towards the automatic computational assessment of enlarged perivascular spaces on brain magnetic resonance images: a systematic review. *J. Magn. Reson. Imag.* **38**(4), 774–785 (2013)
21. Wardlaw, J.M., et al.: Mechanisms of sporadic cerebral small vessel disease: insights from neuroimaging. *Lancet Neurol.* **12**(5), 483–497 (2013)
22. Wardlaw, J.M., et al.: Perivascular spaces in the brain: anatomy, physiology and pathology. *Nature Rev. Neurol.*, 1–17 (2020)